Table 3. Atomic displacement amplitudes (Å). Numbers in parentheses are last-digit uncertainties.

Atom	Direction	Phase	Amplitude	
			First harmonic	Second harmonic
Bi	$u(\mathbf{a})$	0	−0.39(1)	0.15(1)
	$u(\mathbf{b})$	90	0.04(1)	−0.02(2)
	$u(\mathbf{c})$	90	0.19(1)	−0.06(1)
Sr	$u(\mathbf{a})$	0	−0.24(1)	0.15(2)
	$u(\mathbf{b})$	90	−0.03(3)	−0.05(6)
	$u(\mathbf{c})$	90	0.20(1)	−0.08(2)
Cu	$u(\mathbf{a})$	0	−0.04(1)	0.04(4)
	$u(\mathbf{b})$	90	0.00(3)	0.04(10)
	$u(\mathbf{c})$	90	0.28(1)	−0.04(2)

ment amplitudes reported in Table 3 were not significantly altered in these refinements.

REFERENCES AND NOTES

1. M. A. Subramanian *et al.*, *Science* **239**, 1015 (1988).
2. P. Bordet *et al.*, in *Proceedings of the International Conference on High Temperature Superconductors and Materials and Mechanisms of Superconductivity*, J. Müller and J. L. Olsen, Eds. (North-Holland, Amsterdam, 1988), pp. 623–624.
3. S. A. Sunshine *et al.*, *Phys. Rev. Sect. B* **38**, 893 (1988).
4. J. M. Tarascon *et al.*, *ibid.* **37**, 9382 (1988).
5. V. Petricek, P. Coppens, P. Becker, *Acta Crystallogr. Sect. A* **41**, 478 (1985).
6. P. M. De Wolff, T. Janssen, A. Janner, *ibid.* **37**, 625 (1981).
7. V. Petricek and P. Coppens, *Acta Crystallogr. Sect. A.*, in press.
8. T. M. Shaw *et al.*, *Phys. Rev. B* **37**, 9856 (1988); P. L. Gai and P. Day, *Physica C*, in press.
9. G. Chen and W. A. Goddard III, *Science* **239**, 899 (1988).
10. C. C. Torardi *et al.*, *ibid.* **240**, 631 (1988).
11. M. A. Subramanian *et al.*, *Nature* **332**, 420 (1988).
12. J. D. Fitzgerald *et al.*, *Phys. Rev. Lett.* **60**, 2797 (1988).
13. A. K. Cheetham, A. M. Chippindale, S. J. Hibble, *Nature* **333**, 21 (1988); A. M. Chippindale *et al.*, *Physica C* **152**, 154 (1988).

14. Support of this work by the National Science Foundation (CHE8711736) is gratefully acknowledged.

22 June 1988; accepted 19 July 1988

Neutron Imaging of Laser Fusion Targets

D. RESS, R. A. LERCHE, R. J. ELLIS, S. M. LANE, K. A. NUGENT

A long-term goal of inertial-confinement fusion research is the generation of energy by imploding capsules containing deuterium-tritium fuel. Progress in designing the capsules is aided by accurate imaging of the fusion burn. Penumbral coded-aperture techniques have been used to obtain neutron images that are a direct measurement of the fusion burn region in the capsules.

NEUTRON IMAGES OF LASER-DRIVEN inertial confinement fusion (ICF) targets were recently obtained at the Nova laser facility of the Lawrence Livermore National Laboratory (LLNL). These images provide a direct measurement of the deuterium-tritium (DT) fusion burn region within a compressed target. We describe the imaging system, review the physics of neutron emission by ICF implosions, present two examples of the neutron images, and compare the experimental results with theoretical predictions.

A major goal of ICF research is the generation of energy by imploding targets containing DT fuel. Efficient energy production requires that such a target produce 100 times more energy than is used to drive the implosion. This high gain can be obtained by compressing the fuel in a particular fashion (*1*). Most of the fuel is strongly compressed to a density $\rho > 200$ g/cm^3 at the relatively low ion temperature $\theta_i \approx 1$ keV. At the center of this highly compressed fuel is a much smaller "hot spot" containing about 1% of the fuel mass at a much lower density ($\rho > 30$ g/cm^3) but higher temperature ($\theta_i \approx 4$ keV). Fusion is initiated in this hot spot, producing a thermonuclear burn wave that propagates into the surrounding cooler fuel.

Previous diagnostic techniques do not diagnose hot-spot formation and ignition. X-ray emission, which is the basis for many widely used ICF diagnostics, depends on the spatial and temporal profiles of the plasma density, ionization state, and electron temperature. During an ICF implosion, the electron and ion temperatures can be quite different, and mixing of target components leads to complicated spatial variations in the ionization state. Thus, an x-ray image provides information about the spatial structure of several complex processes within the target that are not directly related to the fusion reaction. A neutron image, on the other hand, provides a direct measurement of the spatial extent of the fusion reaction. Furthermore, in advanced targets that achieve high compression, most reaction products and x-rays are absorbed within the target; only the neutrons escape. Neutron imaging, therefore, has long been recognized for its potential to unambiguously diagnose both compression and hot-spot formation in the burning fuel (*2*).

ICF experiments at Nova will soon focus on the physics of hot-spot formation. Because of the limited energy of the Nova laser, these experiments will create implosions that contain only the hot-spot region and do not ignite. For such targets, the neutron emission region is less than 25 μm in diameter with a yield (neutrons produced per implosion) of 10^{11}. Conventional pinhole imaging is not sensitive enough to produce neutron images of such targets. Penumbral imaging, a technique previously used to obtain x-ray images of laser-produced plasmas (*3*), has been suggested as a more efficient method to image neutrons emitted by ICF targets (*4*). Our recent numerical and theoretical calculations verified the feasibility of neutron penumbral imaging. Here we report experimental results obtained with a preliminary neutron imaging system for ICF.

Penumbral imaging is a coded-aperture-imaging technique. It is conceptually similar to pinhole imaging with the essential difference that the aperture is larger than the source. The geometry of penumbral imaging is shown in Fig. 1. The image produced consists of a uniform bright region surrounded by a partially illuminated penumbra. All the spatial information about the source is encoded in this penumbra.

The neutron penumbral imaging system

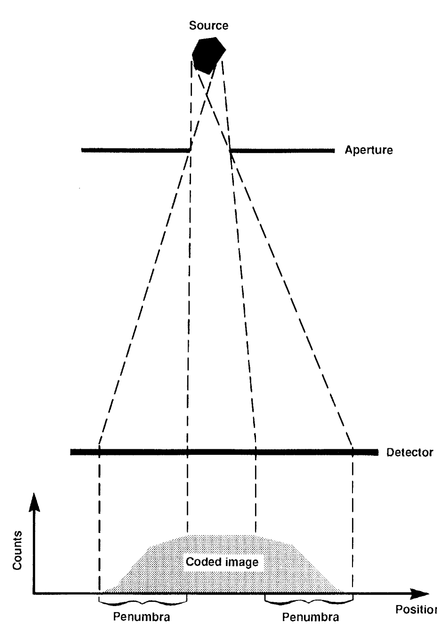

Fig. 1. Geometry of the penumbral imaging process.

D. Ress, R. A. Lerche, R. J. Ellis, S. M. Lane, Lawrence Livermore National Laboratory, P.O. Box 808, Livermore, CA 94550.
K. A. Nugent, The University of Melbourne, School of Physics, Parkville, Victoria, Australia 3052.

consists of an aperture, a detector, and appropriate software to deconvolve the coded image. To block the penetrating 14-MeV neutrons, the aperture must be several centimeters thick. Fabrication is greatly simplified, as compared to a pinhole aperture, because the diameter of the penumbral aperture is large compared to the desired resolution; see Fig. 2. The neutron detector is a circular array of 1240 elements. Each element is a 10-cm-long rod with a square cross section 2 mm on a side, and fabricated from plastic scintillator material. Each element produces blue light in proportion to the deposited neutron energy. The coded image recorded by the detector must be deconvolved to produce an image of the neutron source. Deconvolution requires precise knowledge of the neutron aperture point-spread function; this information is obtained during the aperture fabrication process by mechanical characterization. The deconvolution is carried out in the Fourier transform domain with a parametric Wiener filter (*5*).

The ICF targets were spherical glass shells, 1 mm in diameter with walls 2 μm in thickness and filled with 25 atmospheres of equimolar DT gas (*6*). To achieve an implosion, a target is irradiated by the Nova laser (*7*). The laser consists of two five-beam clusters that produce a complex, asymmetric illumination pattern on the target. More than 20 kJ of 351-nm light is focused onto the target in a 1-ns temporally square pulse. Unlike the more optimal designs discussed previously, these targets do not produce strong fuel compression, but instead generate large neutron yields by achieving a high ion temperature (9 keV). Radial convergence of the glass shell is less than 3, thus producing a relatively large neutron source region compatible with the resolution of our imaging system. Neutron yields varied from 2.0×10^{12} to 1.2×10^{13}, and the duration of the fusion burn was measured with photoconductive devices (*8*) to be in the range 300 to 400 ps full-width at half-maximum (FWHM).

The neutron image provides a measurement of the spatial profiles of important physical parameters within the fuel. Consider the DT fusion reaction

$$D + T \rightarrow {}^{4}He(3.5\ MeV) + n(14.1\ MeV) \quad (1)$$

The fusion reaction rate per differential volume of the fuel region is

$$R_{DT} = n_D n_T \langle \sigma v \rangle_{DT} \quad (2)$$

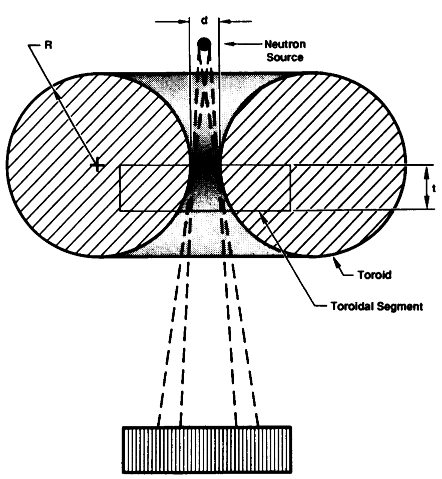

Fig. 2. Principle of the toroidal segment aperture. To simplify the image reconstruction process, the point-spread function of the aperture must be reasonably isoplanatic. To achieve such a point-spread function with an aperture thick enough to effectively block neutrons requires a three-dimensionally tapered aperture. A particularly satisfactory taper is a toroid where the radius of curvature (minor radius of the toroid) R is much greater than the aperture thickness t. A practical realization of this concept utilizes a segment of the toroid determined by the maximum size of the source and the source-aperture distance. The results presented here were obtained with an aperture 6.1 cm long, with a minimum diameter d of 407 μm and a radius of curvature of 19.5 m.

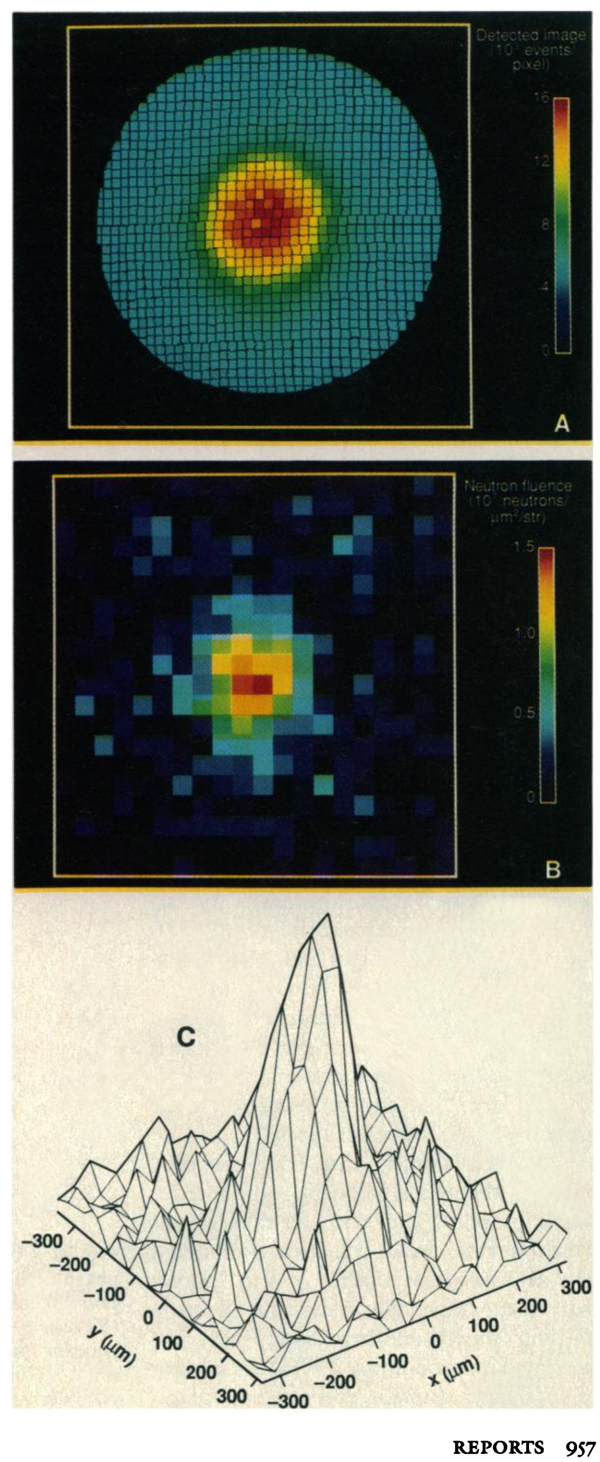

Fig. 3. Neutron image of a high-yield target with conventional illumination. (**A**) Coded image of the target in false color. (**B** and **C**) The unfolded neutron image. The unfolded image is obtained from the coded image by deconvolution in the Fourier transform domain with a Wiener filter. For a penumbral image, the transform of the point-spread function has many zeroes, and the filter serves to deemphasize the discrete spatial-frequency components in the coded image that lie close to these zeroes.

where $n_{D(T)}$ is the deuterium (tritium) ion density, and $\langle \sigma v \rangle_{DT}$ is the DT fusion reaction rate averaged over a Maxwellian distribution. The reaction rate is a complicated function of the ion temperature, θ_i; for these targets, $\langle \sigma v \rangle_{DT}$ increases approximately as $\theta_i^{5/2}$. For an equimolar mixture of deuterium and tritium, the total ion density $n_i = 2n_D = 2n_T$. The average neutron production across a pixel area is

$$\langle R_{DT} \rangle = \frac{1}{\Delta s^2 \tau_b} \int\int dA\ dt\ R_{DT} \propto \int\int dA\ dt\ n_i^2 \theta_i^{5/2} \quad (3)$$

where $\int dA = \Delta s^2$ is the pixel element area referred to the source plane, and τ_b is the FWHM neutron emission time. The neutron image records the line average of $\langle R_{DT} \rangle$ from which the spatial profile of the neutron production rate can be obtained by Abel inversion with an appropriate symmetry assumption. Thus, the neutron image depends on the spatial profiles of both the ion temperature and density.

Images were obtained of targets that produce the typical yield of 10^{13}. The images are quite similar; one is presented in Fig. 3, A through C. Figure 3A shows a false color image of the coded neutron image. Approximately 15,000 neutrons interact in each scintillator element within the central bright region of the image. Figure 3, B and C, show the unfolded neutron image. Pixel size is 35 μm, and the two-point spatial resolution is approximately 80 μm. The neutron burn region is slightly elliptical, as expected from the laser illumination nonuniformity, with an average FWHM diameter of 150 μm. Signal-to-noise ratio for the peak signal level is estimated to be better than 10.

In another experiment, we attempted to manipulate the shape of the neutron source region by changing the uniformity of the laser illumination. The beams were aimed to preferentially heat opposite sides of the target, producing an extremely nonuniform drive. A reduced yield of 3.0×10^{12} neutrons was produced. The resulting neutron image is larger, with a more complicated shape. At the 70% contour level the image is elliptical with the major axis oriented vertically, as expected, and at lower levels the image has several distinct lobes.

A detailed hydrodynamic computer code provides theoretical modeling of laser-fusion implosions. The computer calculations, which assume exact spherical symmetry, give neutron yields a factor of 3 to 4 larger than is experimentally measured. Neutron imaging shows another discrepancy: the simulated neutron image FWHM is a factor of 15 smaller than the experimental image, see Fig. 4, A and B. The sharp peaking of the simulated neutron image is due to a brief, large rise in density at the center of the target, see Fig. 4C. This strong compression

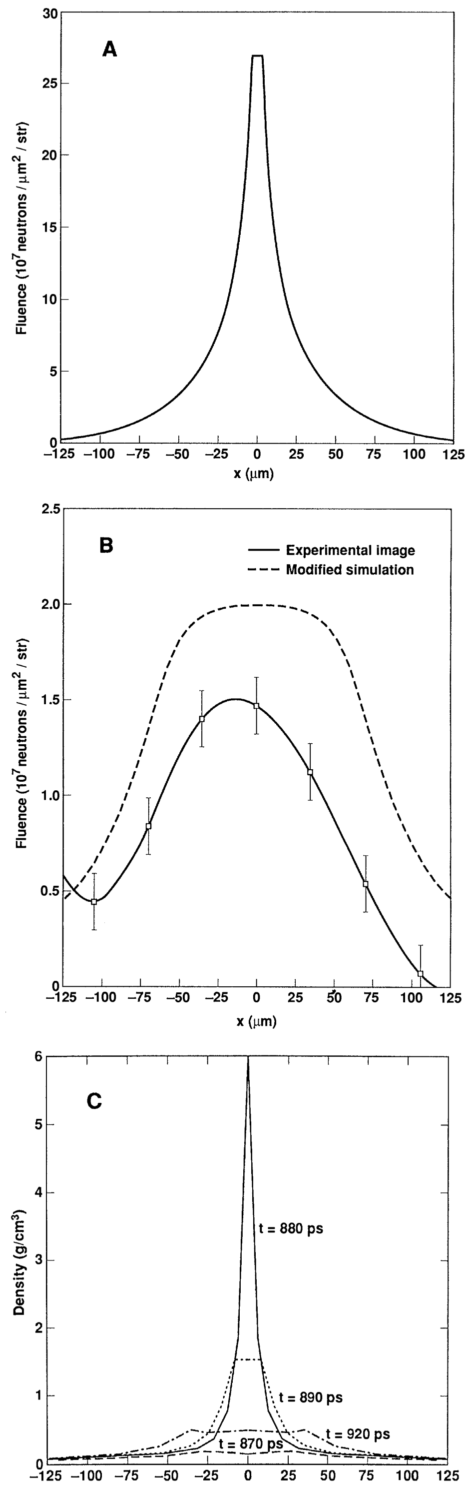

Fig. 4. Comparison of the measured neutron image with the results of a hydrodynamic computer simulation: (**A**) simulated neutron image; (**B**) overlay of x-axis line out of the experimental neutron image with a simulated neutron image ignoring the first 50 ps of neutron emission; and (**C**) overlay of calculated density profiles.

occurs during the first 50 ps of neutron emission, and is associated with the final convergence of a spherical shock wave produced by the simulated laser drive. In the actual experiment, however, the laser illumination is highly asymmetric, and may launch a strongly distorted shock front that does not converge neatly at the target center, producing a lower density compressed region that is spatially and temporally broadened from the one-dimensional code prediction. This hypothesis is also supported by the neutron emission time meausrements, which give a FWHM burn width a factor of 2 to 3 larger than simulation results.

Thus, two-dimensional effects reduce the strong neutron emission from the very center of the target. We have illustrated this effect by producing a simulated neutron image that ignores the first 50 ps of neutron emission. The result, also shown in Fig. 4B, is a good match to the experiment. Moreover, the neutron yield corresponding to this portion of the burn is roughly the same as that produced by the experiment.

Information from the preliminary neutron imaging diagnostic is already providing insight into the physics of laser-fusion implosions. The imaging system resolution and sensitivity can be improved through changes in the aperture and detector. Future efforts will attempt to achieve a two-point resolution of better than 10 μm to allow imaging of targets that reach a high radial convergence and produce yields of 10^{11} neutrons or less. The enhanced imaging system will be a valuable diagnostic tool for ICF research.

REFERENCES AND NOTES

1. J. Nuckolls, L. Wood, A. Thiessen, G. Zimmerman, *Nature* **239**, 139 (1972).
2. D. T. Attwood *et al.*, in *Laser Interaction and Related Plasma Phenomena*, H. J. Schwarz, H. Hora, M. J. Lubin, B. Yaakobi, Eds. (Plenum, New York, 1981), vol. 5, pp. 423–463.
3. K. A. Nugent and B. Luther-Davies, *Optics Comm.* **49**, 393 (1984).
4. ______, *J. Appl. Phys.* **58**, 2508, (1985).
5. R. C. Gonzalez and P. Wintz, *Digital Image Processing* (Addison-Wesley, Reading, PA, 1977).
6. Targets for these experiments were provided by the LLNL Target Fabrication Group and KMS Fusion, Inc., P.O. Box 1567, Ann Arbor, MI.
7. E. M. Campbell, J. T. Hunt, E. S. Bliss, D. R. Speck, R. P. Drake, *Rev. Sci. Instrum.* **57**, 2101 (1986).
8. D. R. Kania *et al.*, *IEEE Trans. Nucl. Sci.* **35**, 387 (1988).
9. We acknowledge the efforts of the many scientists and technicians at LLNL who contributed to this effort: C. Bennett, J. Cardinal, J. Clements, D. Goosman, R. Griffith, R. Horton, B. Jones, H. Medecki, D. H. Munro, C. Sanner, J. Smith, and C. Wang. We are also grateful to the Nova Operations and Target Fabrication groups, and the Material Fabrication Division for their excellent support in completing this set of experiments.

6 April 1988; accepted 23 June 1988